Journal of Integrative Neuroscience

J. Integr. Neurosci. **2025**; 24(10): 43900
https://doi.org/10.31083/JIN43900

Original Research

Poliumoside Alleviates Neuroinflammation and Oxidative Stress After Spinal Cord Injury by Activating the PI3K/AKT/mTOR Signaling Pathway

Qianqiu Li[1,2], Hongxiang Hong[1], Guanhua Xu[1,3], Mingjie Xia[3], Tianyi Wang[1,2], Zheng Zhou[1,2], Jiale Huang[1,2], Qihao Fu[1,2], Zhiming Cui[1,3,*]

[1]Department of Spinal Surgery, The Second Affiliated Hospital of Nantong University, 226001 Nantong, Jiangsu, China
[2]Medical School of Nantong University, 226001 Nantong, Jiangsu, China
[3]Research Institute for Spine and Spinal Cord Disease of Nantong University, 226001 Nantong, Jiangsu, China
*Correspondence: czmspine@ntu.edu.cn (Zhiming Cui)
Academic Editors: Nuno A. Silva and Bettina Platt
Submitted: 16 June 2025 Revised: 16 September 2025 Accepted: 19 September 2025 Published: 29 October 2025

Abstract

Background: Spinal cord injury (SCI) constitutes a profoundly debilitating neurological disorder precipitating motor and sensory function impairment. Curtailing microglia-driven neuroinflammation alongside oxidative stress proves indispensable for efficacious SCI patient management. Poliumoside (POL), a phenylethanoid glycoside molecule, manifests anti-inflammatory, antioxidant, and neuroprotective capacities. Nevertheless, documentation concerning its SCI therapeutic efficacy remains sparse. **Methods**: Systemic drug toxicity for two POL dosages (15 mg/kg, 30 mg/kg) was evaluated across multiple organs. An SCI murine model was generated employing Allen's technique. Mice received random assignment into sham, SCI, and SCI+POL cohorts. Intraperitoneal POL administration ensued for 7 consecutive days post-trauma. Histological staining probed tissue and cellular alterations. Functional recuperation was assessed via the Basso Mouse Scale (BMS), hindlimb flexion scoring, and footprint examination. RNA sequencing (RNA-seq) explored POL's therapeutic impact within SCI. Immunofluorescence detected the axonal marker neurofilament 200 (NF200), myelin marker myelin basic protein (MBP), and the glial scar indicators ionized calcium-binding adapter molecule 1 and glial fibrillary acidic protein (IBA1, GFAP); Western blot (WB) identified the nerve growth-associated protein 43 (GAP43). WB and immunofluorescence quantified inflammatory and oxidative stress markers. POL's regulatory function within the phosphatidylinositol 3-kinase (PI3K)/protein kinase B (AKT)/mechanistic target of rapamycin (mTOR) cascade was scrutinized both *in vivo* and *in vitro*. **Results**: POL intervention induced no systemic organ toxicity. POL-treated mice exhibited pronounced locomotor function enhancement, diminished neuronal tissue depletion, elevated neuronal survival, and attenuated demyelination. RNA-seq analysis illuminated POL's SCI therapeutic mechanism linkage to axonal regeneration, the phosphatidylinositol signaling apparatus, and the neuronal framework. POL concurrently attenuated glial scar formation and potentiated axonal and myelin regeneration. Mechanistically, POL suppressed pro-inflammatory cytokines and oxidative stress mediators while activating the PI3K/AKT/mTOR pathway. **Conclusions**: POL mitigated murine spinal cord injury-induced neuroinflammation and oxidative stress through PI3K/AKT/mTOR signaling pathway activation. Furthermore, POL treatment contracted the glial scar expanse within the injury epicenter and fostered axonal regeneration coupled with myelin regeneration. Consequently, POL enhances post-SCI motor function and accelerates neural function restoration.

Keywords: axon; neuroinflammation; oxidative stress; PI3K; poliumoside; spinal cord injury

1. Introduction

Spinal cord injury (SCI) arises from direct or indirect mechanical trauma, precipitating partial sensation or motor function forfeiture below the lesion site, variable disability levels, or complete paralysis plus diverse complications [1]. Its elevated disability incidence and grave complications impose considerable socioeconomic encumbrance [2]. SCI pathophysiology encompasses primary mechanical trauma and secondary damage. Primary injury stems from the initial traumatic spinal cord assault, inflicting irreversible neural tissue structural compromise. Subsequently, ischemic conditions and edematous manifestations subsequent to hemorrhagic events and vascular thrombosis intensify the primary insult, culminating in progressive tissue deterioration and functional impairment [3]. Secondary SCI injury hallmarks encompass neuroinflammation, oxidative stress, and demyelination, exacerbating tissue destruction while suppressing axonal regrowth within the lesion zone [4]. Neuroinflammation proves instrumental in post-SCI secondary injury, chiefly orchestrated by central nervous system (CNS) microglia [5].

Microglia, the CNS's resident immune sentinels, crucially uphold neural equilibrium during physiological states [6]. Post-SCI, however, microglia undergo swift activation responding to pathological stimuli, adopting a pro-inflammatory configuration that liberates excessive inflammatory mediators: tumor necrosis factor-

α (TNF-α), interleukin-1β (IL-1β), interleukin-6 (IL-6), cyclooxygenase-2 (COX-2), and inducible nitric oxide synthase (iNOS) [7]. This reactive microglial phenomenon aggravates secondary harm by advancing neurotoxicity, breaching the blood-spinal cord barrier, and impeding axonal regeneration. Notably, neuroinflammatory-driven excessive neuroglial scar accumulation and myelin depletion obstruct axonal regrowth [8]. Furthermore, pro-inflammatory mediator overproduction may instigate inflammatory cascade reactions, subsequently driving pathological intracellular reactive oxygen species (ROS) overgeneration. ROS-induced oxidative stress further impairs neuronal biological functionality [9]. Concurrently, microglia bidirectionally modulate their phenotypes via autocrine signaling through concurrent pro- and anti-inflammatory cytokine liberation, while exerting paracrine influences on injury-associated neurons and astrocytes [10]. Therefore, inhibiting the injury caused by neuroinflammation and oxidative stress mediated by microglia is crucial for improving motor function after SCI and promoting neural function repair.

Axonal and neural regeneration in the CNS represent a complex yet pivotal biological process critical for functional recovery following SCI, but remain severely limited in adult mammals due to multifaceted intrinsic and extrinsic barriers [11]. The regenerative potential of injured axons depends on the reactivation of growth cones, which requires coordinated regulation of cytoskeletal dynamics through Ras homologous (Rho) GTPases and activation of pro-regenerative signaling pathways including phosphatidylinositol 3-kinase (PI3K)/protein kinase B (AKT)/mechanistic target of rapamycin (mTOR) and rat sarcoma virus oncogene (Ras)/rapidly accelerated fibrosarcoma oncogene (Raf)/mitogen-activated protein kinase/extracellular signal-regulated kinase kinase (MEK)/extracellular signal-regulated kinase (ERK), collectively enhancing the neuron's intrinsic growth capacity [12].

Poliumoside (POL, Fig. 1A) is a natural phenylethanoid glycoside compound [13]. Investigations reveal substantial anti-inflammatory properties, antioxidative capability, anti-apoptotic action, and neuroprotective potency [14,15], with POL mitigating oxidative impairment and pulmonary inflammation within TNF-α-induced acute lung injury cellular paradigms through nuclear factor erythroid 2-related factor 2 (Nrf2) and nuclear factor kappa-light-chain-enhancer of activated B cells (NF-κB) pathway modulation [16]. In recent years, the therapeutic potential of POL treatment in neurological diseases has attracted much attention. For instance, POL treatment has been shown to alleviate cognitive dysfunction in Alzheimer's Disease (AD) model rats by inhibiting cell apoptosis, oxidative stress, and neuroinflammation [17]. Separate research identified POL's inhibition of microglia-regulated neuroinflammation and neurotoxicity in cerebral hypoxia-ischemia models via Fstl1-NF-κB pathway suppression [18], while POL governs microglial polarization through selective JAK/STAT3 signaling pathway inhibition, consequently attenuating microglia-mediated neuroinflammation [19]. A related study found that POL, as a fanconi anemia complementation group C (FANCC) agonist, effectively promoted mitochondrial autophagy in astrocytes and inhibits necrotic apoptosis after SCI [20]. Nevertheless, POL's neuroprotective consequences post-SCI alongside its fundamental mechanisms and precise operational modality remain incompletely elucidated.

The PI3K/AKT/mTOR signaling cascade engages multifarious regulatory and effector molecules, operating as a principal governor of diverse CNS neurophysiological phenomena encompassing neuronal cellular expansion, viability, and axonal ontogenesis [21]. PI3K/AKT pathway activation proves particularly consequential within SCI's pathological cascade, since activation delays inflammatory reactions, precludes glial cicatrix formation, and advances functional neurological restitution [22]. Additionally, post-SCI mTOR signaling stimulation exerts multifarious governance across distinct neurobiological processes including axonal reconstitution, neuroinflammatory modulation, and glial scar establishment [23]. Consequently, we probed whether POL intervention modulates the PI3K/AKT/mTOR signaling axis to repress neuroinflammation and oxidative stress while facilitating axonal regeneration after SCI.

2. Materials and Methods

2.1 Animals

Eighty-one female wild-type C57BL/6J mice (8-week-old, 20–30 g) were procured from Nantong University's Animal Center (Nantong, Jiangsu, China). Specimens were maintained under controlled temperature/humidity with 12-hour photoperiods. Breeding and experimental procedures occurred at Nantong's Animal Experiment Center under regulatory compliance. All protocols adhered to ARRIVE (2.0) guidelines with ethical approval from Nantong University's Animal Experiment Ethics Committee (No. S20250318-004). A comprehensive chronological flowchart delineated the experimental design (Fig. 1B).

2.2 SCI Model and Treatments

Anesthesia was induced in the mice via i.p. injection of ketamine (K2753, Sigma-Aldrich, St. Louis, MO, USA) (80 mg/kg). The spinal cord on the T10 vertebrae was struck with a percussion device (68099, RWD Life Science, Shenzhen, China) to produce spinal cord contusion. After impact, the mice still exhibited tail-flick reflexes, and spinal cord hemorrhage was observed in the central region. The mice were placed on a heating pad for recovery. Post-recovery, bilateral hindlimbs showed no an-

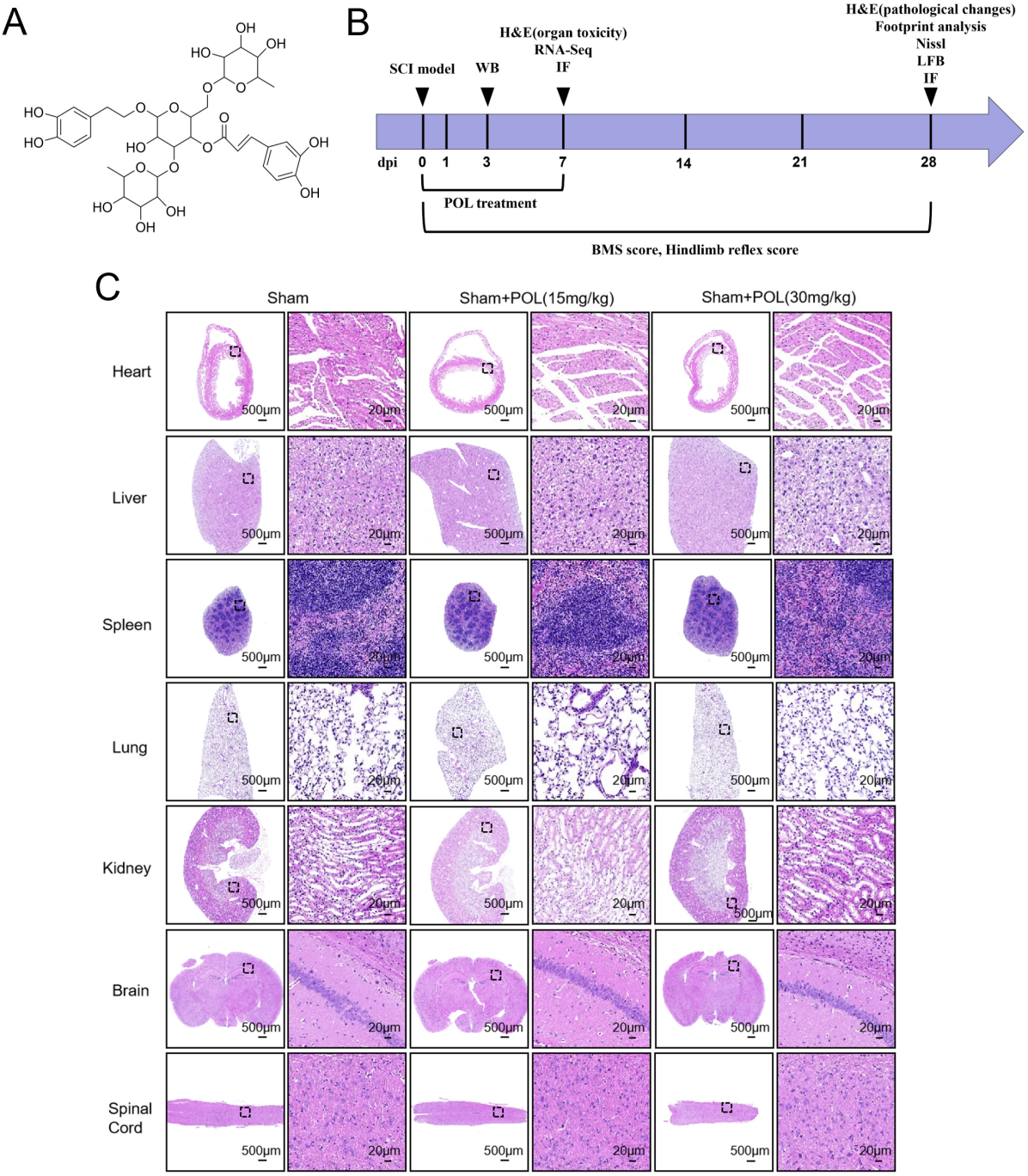

Fig. 1. POL treatment did not induce organ toxicity in SCI mice. (A) POL molecular configuration. (B) Chronological schema for SCI murine interventions and assessments. (C) H&E analysis reveals negligible organic pathology in cardiac, hepatic, splenic, pulmonary, renal, cerebral, or spinal tissues from low/high-dose POL specimens. Scale bars = 500 μm, 20 μm. POL, Poliumoside; SCI, Spinal cord injury; H&E, Hematoxylin-eosin; WB, Western blot; BMS, Basso Mouse Scale; LFB, Luxol Fast blue; dpi, days after injury; IF, Immunofluorescence; RNA-Seq, Ribonucleic Acid Sequencing.

kle joint movement, corresponding to a Basso Mouse Scale (BMS) score of 0, indicating establishment of a successful SCI model. In the sham group, mice underwent laminectomy only, wherein the vertebral laminae were completely removed, followed by sequential suturing of the muscle layer, fascial layer, and skin. For treatment, mice in the SCI group received i.p. injections of POL (HY-N0033, MedChemExpress, Woodbridge, NJ, USA) at doses of 15 mg/kg and 30 mg/kg immediately after successful model establishment and after resuscitation. Subsequent injections were administered every 24 h for 7 consecutive days. Sham and SCI groups received i.p. injection of an equivalent volume

of saline daily. To prevent urinary retention, SCI mice underwent daily assisted bladder expression until recovery of spontaneous voiding function.

2.3 Behavioral Tests

Motor function recovery in SCI mice was assessed using the BMS, hindlimb reflex score, and footprint analysis. To minimize subjective bias, all evaluations were performed by two independent evaluators, blind to group identification, who were familiar with the experimental protocol but not directly involved in the study. (1) BMS score: hindlimb motor function was assessed using the BMS on days 1, 3, 7, 14, 21, and 28 after SCI (days after injury = dpi) [24]; (2) hindlimb reflex score: At 1, 3, 7, 14, 21, and 28 dpi, mic Subsequentlye were suspended at a height of approximately 30 cm for 14 sec. Hindlimb motor function was assessed using the following scoring criteria: 0, Normal; 1, Incomplete hindlimb extension; 2, Hindlimb clasping; 3, Hindlimb paralysis; (3) Footprint analysis: at 28 dpi, mice were tested for gait analysis using dye-marked limbs (red: forelimbs; blue: hindlimbs) on a paper-lined runway. Quantitative assessment of locomotor recovery included measurements of stride length and stride width from the footprints.

2.4 Nissl Staining

After being deeply anesthetized by intraperitoneal injection of ketamine at a dose of 80 mg/kg, mice were euthanized by carbon dioxide asphyxiation to ensure death prior to tissue collection. Subsequently, the abdomen was incised and the diaphragm was punctured to expose the heart. Cold phosphate-buffered saline (PBS, ST476, Beyotime, Shanghai, China) and 4% polyformaldehyde (P6148, Sigma-Aldrich) solution were sequentially injected into the heart. After the perfusion was completed, the damaged central spinal cord segment (1.5 cm in length) was removed and immediately immersed in 4% polyformaldehyde solution for preservation. Then, dehydration treatment was carried out and sections were made using a paraffin sectioning machine (Kedee KD-202A, Hisure, Jinhua, Zhejiang, China). Thin sections of 5 micrometers were cut longitudinally. For the immunofluorescence experiment, the preparation process of the tissue samples was the same as described above. Subsequently, the tissue was stained using the instructions provided by the Nissl staining kit (G1036, Servicebio, Wuhan, Hubei, China) and observed under a microscope (DM2500, Leica, Berlin, Germany). The specific parameters are as follows: Bright field, 4×, exposure time 20 ms.

2.5 Hematoxylin-eosin Staining

Hematoxylin-eosin (H&E) staining was executed employing an H&E staining kit (G1005, Servicebio). Paraffin-embedded spinal cord sections underwent xylene dewaxing (5 min), graduated ethanol rehydration, hematoxylin immersion (5 min), eosin counterstaining (2 min), and acid alcohol differentiation (10 sec) prior to dehydration and mounting. Section evaluation utilized a DM2500 microscope (Leica) under bright-field illumination (4× magnification; 10 ms exposure).

2.6 Luxol Fast Blue Staining

Luxol Fast blue (LFB) staining was performed using the LFB staining kit (G1092, Servicebio). For LFB myelin staining, sections were incubated in 0.1% Luxol Fast Blue for 2 h, differentiated in lithium carbonate for 10 sec until clear gray-white matter contrast was achieved, with microscope (DM2500, Leica) validation of myelin integrity (bright blue signal). The specific parameters are as follows: Bright field, 4×, exposure time 50 ms.

2.7 RNA Sequencing

On the 7th day after SCI, the mice in the SCI and SCI+POL (30 mg/kg) groups were euthanized, and their spinal cords removed. RNA was extracted from the spinal cords using TRIzol reagent (EF0131, YiFeiXue, Nanjing, Jiangsu, China). The cDNA library construction and RNA sequencing were carried out by GeneChem (Shanghai, China). Seven days post-SCI, euthanized SCI and SCI+POL (30 mg/kg) cohort mice underwent spinal cord extraction. RNA isolation employed TRIzol reagent (YiFeiXue). cDNA library preparation and RNA sequencing were executed by GeneChem. Total RNA (1 µg/sample) underwent library construction using the NEBNext® Ultra RNA Library Prep Kit (E7530, New England Biolabs, Ipswich, MA, USA). Poly(A)+ mRNA enrichment utilized oligo(dT)-immobilized magnetic beads, followed by fragmentation in NEBNext® First Strand Buffer (94 °C, 15 min). First-strand cDNA synthesis deployed random hexamers with M-MuLV Reverse Transcriptase; second-strand synthesis employed DNA Polymerase I. After end repair and 3′ adenylation, NEBNext® adaptors were ligated. Size selection (250–300 bp) was performed using AMPure XP beads (A63880, Beckman Coulter, Brea, CA, USA), followed by USER enzyme treatment (37 °C, 15 min) and PCR amplification with Phusion polymerase. Final libraries were quality-controlled on an Agilent 2100 Bioanalyzer (G2939A, Agilent Technologies, Santa Clara, CA, USA). Transcript quantification derived from fragments per kilobase per million mapped reads. Differential gene expression screening implemented the DESeq2 algorithm. Genes exhibiting adjusted p-values < 0.05 alongside fold changes exceeding 2 underwent classification as differentially expressed, proceeding to subsequent enrichment analyses.

2.8 Western Blot

Western blot (WB) employed a total protein extraction kit (KGP2100, KeyGEN BioTECH, Nanjing, Jiangsu, China) to isolate proteins from murine spinal cords and microglial cells separately. Protein concentration quantifica-

tion utilized an enhanced BCA assay kit (P0012, Beyotime, Shanghai, China). Prior to electrophoresis, gel formulation deployed a polyacrylamide gel electrophoresis (PAGE) gel rapid preparation kit (PG211, Epizyme, Shanghai, China). Protein transfer onto polyvinylidene fluoride (PVDF) membranes (IPVH00010, Millipore, Billerica, MA, USA) occurred via rapid transfer solution (35 min duration). Post-transfer, PVDF membranes underwent ddH_2O rinsing followed by immersion in freshly constituted 5% skimmed milk (1160GR500, BioFroxx, Guangzhou, Guangdong, China) for 1.5 hours at ambient temperature to effect blocking. Subsequently, membranes underwent primary antibody incubation overnight at 4 °C, succeeded by secondary antibody co-incubation at room temperature for 1 hour the ensuing day. Antibody specifications appear in Table 1. Protein signal acquisition employed an automated chemiluminescence imaging platform (Tanon 5200, Tanon Science & Technology, Shanghai, China), with quantification executed via ImageJ software (Version 1.54r, NIH, Bethesda, MD, USA).

2.9 Immunofluorescence Staining

For the spinal cord paraffin sections, the first step is to deparaffinize and hydrate, then use the sodium citrate fixative solution (P0081, Beyotime) for thermal antigen retrieval, followed by adding the endogenous peroxidase strong blocking solution (P0100B, Beyotime) and incubating at room temperature for 30 min. For the cell slide sections, the spinal cord paraffin sections and cell slide sections start to be consistent from the following experimental steps. For immunofluorescence, specimens received immunostaining blocking solution (P0102, Beyotime) incubated at ambient temperature for 1 hour. Primary antibody application preceded overnight incubation at 4 °C. The subsequent day witnessed incubation with corresponding fluorescent secondary antibodies at ambient temperature for 1 hour (under light-restricted conditions). Antibody particulars are cataloged in Table 1. 4′,6-Diamidino-2-phenylindole (DAPI, G1012, Servicebio) solution application ensued until complete specimen coverage, followed by 10-minute ambient incubation. Conclusively, anti-fluorescence quenching mounting medium (G1401, Servicebio) was applied before coverslip-mediated sample sealing. The sections were observed with a microscope (DM2500, Leica). The specific parameters are as follows: Fluorescence imaging, 20×, DAPI: excitation filter: 360/40 nm, emission filter: 460/50 nm, exposure time: 80 ms; FITC: excitation filter: 480/30 nm, emission filter: 460/50 nm, exposure time: 150 ms; Tetramethylrhodamine isothiocyanate (TRITC): excitation filter: 560/25 nm, emission filter: 630/60 nm, exposure time: 220 ms. Then use the measurement tools in ImageJ to quantify the fluorescence intensity, and ultimately compare the fluorescence levels among different experimental groups.

2.10 Cell Culture and Treatments

BV-2 microglial cells (CL-0493, Wuhan Pricella Life Science & Technology, Wuhan, Hubei, China) were sustained in Dulbecco's Modified Eagle Medium (DMEM; KGM12800, KeyGEN, Nanjing, Jiangsu, China) enriched with 10% fetal bovine serum (FBS; 10099141, Gibco, Waltham, MA, USA) and 1% Penicillin-Streptomycin (15140122, Gibco, Grand Island, NY, USA) under 37 °C/5% CO_2 conditions. The microglial BV-2 cell line was authenticated by short tandem repeat (STR) profiling. Mycoplasmic contamination was absent in the authenticated BV2 line by using both PCR-based and colorimetric assay methods. To establish a neuroinflammatory paradigm, cultures received 20 µM POL (HY-N0033, MedChemExpress, Woodbridge, NJ, USA) pretreatment for 24 hours preceding 1 µg/mL lipopolysaccharide (LPS; L2880, Sigma-Aldrich) stimulation for 6 hours.

2.11 Cell Viability Detection

Cellular viability underwent quantification via Cell Counting Kit-8 (CCK-8; C6005, NCM Biotech, Suzhou, Jiangsu, China). BV-2 progeny were subjected to 5 µM, 10 µM, 20 µM, 40 µM, and 80 µM POL exposure for 6 hours, succeeded by CCK-8 incubation (10 µL, 2 hours). Absorbance measurements (450 nm) utilized a Biotek microplate reader (Synergy H1, Agilent BioTek, Winooski, VT, USA), with untreated specimens representing 100% viability controls.

2.12 Molecular Docking

The 3D structure of Poliumoside was obtained from PubChem in structured data file (SDF) format and converted to mol2 format using OpenBabel (Version 2.4.1, Open Babel development community). Protein targets (PI3K, AKT, and mTOR) were retrieved from the UniProt database, and their protein data bank (PDB) files were processed in PyMOL (Version 2.5.x, Schrödinger, LLC, New York, NY, USA) to remove water molecules and ligands. Molecular docking was performed using AutoDock Vina (v1.5.6, Olson Lab, La Jolla, CA, USA), where protein structures were hydrogenated, and the ligand (POL) was optimized by assigning charges and rotatable bonds. Molecular docking positioned the search box centrally within the active site. Optimal binding conformations were selected according to docking scores (kcal/mol) and visualized via PyMOL. We considered the target proteins (PI3K, AKT, and mTOR) to exhibit strong binding affinity with Poliumoside when the binding energy was <-7 kcal/mol.

2.13 Statistical Analyses

Statistical analyses deployed GraphPad Prism (Version 10.4.1, GraphPad Software, San Diego, CA, USA). Data represent mean $\pm$ SD from $\geq$3 autonomous replicates. Intergroup comparisons employed one-way ANOVA with Tukey's post hoc analysis ($\geq$3 cohorts). Statistical significance threshold: $^*p < 0.05$.

Table 1. Antibodies information.

Antibodies name #Cat. No	Source	Species	Application	Dilution rate
iNOS Polyclonal antibody #22226-1-AP	Proteintech	Rb	WB, IF	1:1000, 1:500
COX2/Cyclooxygenase 2/PTGS2 Monoclonal antibod #66351-1-Ig	Proteintech	Ms	WB, IF	1:1000, 1:200
TNF-alpha Monoclonal antibody #60291-1-Ig	Proteintech	Ms	WB, IF	1:1000, 1:200
IL-1 beta Polyclonal antibody #26048-1-AP	Proteintech	Rb	WB, IF	1:1000, 1:200
IL-6 Rabbit pAb#500286	Zenbio	Rb	WB, IF	1:1000, 1:150
NOX2 Polyclonal antibody #19013-1-AP	Proteintech	Rb	WB	1:2000
NOX4 Polyclonal antibody #14347-1-AP	Proteintech	Rb	WB, IF	1:2000, 1:500
AKT Polyclonal antibody #10176-2-AP	Proteintech	Rb	WB	1:1000
Phospho-AKT(Ser473) Monoclonal antibody #66444-1-Ig	Proteintech	Ms	WB	1:1000
MBP Polyclonal antibody #10458-1-AP	Proteintech	Ms	WB, IF	1:1000, 1:200
IBA1 Polyclonal antibody #10904-1-AP	Proteintech	Rb	IF	1:300
Phospho-PI3 Kinase p85/p55 (Tyr467/Tyr199) Rabbit pAb#341468	Zenbio	Rb	WB	1:1000
PI3 Kinase p85 alpha (1C8) Mouse mAb #251221	Zenbio	Ms	WB	1:1000
Phospho-mTOR (Ser2448) Antibody #2971	CST	Rb	WB	1:1000
mTOR Monoclonal antibody #66888-1-Ig	Proteintech	Ms	WB	1:1000
GFAP(GA5) Mouse mAb #3670	CST	Ms	IF	1:600
Neurofilament-H (E7Z7G) Rabbit mAb #30564	CST	Rb	IF	1:200
ActivAbTMAnti-GAP43 Monoclonal Antibody #K200056M	Solarbio® LIFE SCIENCES	Ms	WB	1:2000
Beta Actin Monoclonal antibody #66009-1-Ig	Proteintech	Ms	WB	1:10,000
Goat Anti-Mouse IgG Secondary antibody (H + L), HRP # YFSA01	YIFEIXUE BioTech	Goat	WB	1:10,000
Goat Anti-Rabbit IgG Secondary antibody (H + L), HRP # YFSA02	YIFEIXUE BioTech	Goat	WB	1:10,000
Alexa Fluor® 594 AffiniPure Fab Fragment Goat Anti-Rabbit IgG (H + L) #111-587-003	Jackson ImmunoResearch	Goat	IF	1:500
Alexa Fluor® 488 AffiniPure Fab Fragment Goat Anti-Rabbit IgG (H + L) #111-547-003	Jackson ImmunoResearch	Goat	IF	1:500
Alexa Fluor® 594 AffiniPure F(ab')2 Fragment Goat Anti-Mouse IgG (H + L) #115-586-003	Jackson ImmunoResearch	Goat	IF	1:500
Alexa Fluor® 488 AffiniPure F(ab')2 Fragment Goat Anti-Mouse IgG (H + L) #115-546-003	Jackson ImmunoResearch	Goat	IF	1:500

®: the registered trademark; #: the antibody number. Abbreviations: iNOS, inducible Nitric Oxide Synthase; COX-2, Cyclooxygenase-2; TNF-α, Tumor Necrosis Factor-α; IL-1β, Interleukin-1 β; IL-6, Interleukin-6; NOX-2, Neutrophil Cytosol Factor 1; NOX-4, Nicotinamide Adenine Dinucleotide Phosphate Oxidase 4; AKT, Protein Kinase B; PI3 Kinase, Phosphatidylinositol 3-Kinase; mTOR, mechanistic Target Of Rapamycin; MBP, Myelin Basic Protein; IBA1, Ionized calcium-binding adapter molecule 1; GFAP, Glial Fibrillary Acidic Protein; IgG, Immunoglobulin G; Rb, Rabbit; Ms, Mouse.

3. Results

3.1 POL Treatment Did Not Induce Organ Toxicity in SCI Mice

Histopathological interrogation of principal organs (brain, spinal cord, heart, liver, spleen, lung, kidney) via H&E staining. Murine subjects received POL (15 or 30 mg/kg) across seven days. Treated cohorts manifested no significant pathological deviations relative to controls, indicating absent POL-induced organic toxicity at examined dosages (Fig. 1C).

3.2 POL Treatment Alleviated Pathological Changes and Improved Motor Function After SCI

To evaluate the therapeutic effects of POL treatment on motor function recovery in SCI mice, we used BMS scoring, hindlimb reflex assessment, and footprint analysis. POL-treated SCI mice demonstrated significantly higher BMS scores than did untreated SCI controls, with particularly notable improvements at 21 and 28 dpi ($p < 0.05$) (Fig. 2A). At 28 dpi, these cohorts additionally manifested diminished hindlimb reflex scores ($p < 0.05$) (Fig. 2B). Plantar imprint analysis disclosed SCI mice administered 15 mg/kg or 30 mg/kg POL exhibited greater anteroposterior stride dimensions and lateral base spans versus SCI counterparts (Fig. 2C), cumulatively denoting augmented locomotor restitution. Particularly, stride magnitude in SCI+POL (30 mg/kg) specimens substantially exceeded SCI group measurements ($p = 0.0021$) (Fig. 2D,E). To evaluate POL's neuropreservative capacities, histological examinations (H&E, Nissl, LFB staining) were conducted at 28 dpi. H&E analysis demonstrated POL administration significantly contracted neural lesion areas dose-dependently ($p = 0.005$) (Fig. 2F,G). LFB staining confirmed that POL treatment attenuated demyelination at the lesion site, particularly at the 30 mg/kg dose ($p = 0.0005$) (Fig. 2H,I). Nissl staining revealed that while SCI caused extensive neuronal death in and around the injured area, the 30 mg/kg POL treatment preserved significantly more surviving neurons ($p = 0.0016$) (Fig. 2J,K). Based on these findings, we selected the dose of 30 mg/kg POL for subsequent experiments.

3.3 POL Treatment Modulated Gene Expression and Regulated Axon Regeneration-associated Pathways After SCI

To further elucidate POL's mechanistic action in SCI intervention, transcriptomic interrogation was conducted. Sequencing outcomes delineated 28,940 differentially expressed genes distinguishing SCI cohorts from SCI+POL counterparts, comprising 1194 substantially upregulated and 1966 markedly downregulated genes ($p \leq 0.05$, $|\log_2\text{FoldChange}| \geq 0$; Fig. 3A). The volcano plot analysis identified three significantly downregulated genes, with *Scn10a* ($p = 9.68 \times 10^{-12}$) and *Mrgprd* ($p = 4.83 \times 10^{-9}$) showing the most pronounced downregulation, both of which are functionally associated with neuropathic pain. Additionally, *Igf1r* ($p = 0.000441$), a target gene implicated in axonal regeneration, was also significantly downregulated. Kyoto encyclopedia of genes and genomes (KEGG) enrichment analysis prominently implicated inflammation-associated signaling cascades, notably the PI3K/AKT/mTOR axis, ras-proximate 1 (Rap1) signaling cascade, and Ras signaling pathway (Fig. 3B). Gene ontology (GO) enrichment evaluation postulated POL's principal biological functionalities pertain to axonal reconstitution post-spinal cord injury (Fig. 3C). Reactome enrichment scrutiny further substantiated POL's predominant involvement in neuronal system-relevant biological processes following SCI (Fig. 3D). Consequently, transcriptomic evidence directed subsequent investigation toward POL's effects on neuroinflammation, axonal regeneration, and PI3K/AKT/mTOR signaling modulation.

3.4 POL Treatment Enhanced Axon Regeneration and Myelin Repair While Reducing Glial Scar After SCI

Following spinal cord injury, axonal reconstitution and myelin sheath remodeling constitute pivotal processes for neural function restoration. Our investigation documented significantly elevated neurofilament 200 (NF200) axonal density within lesion areas of POL-treated specimens versus SCI controls through immunofluorescence, indicating enhanced axonal regeneration ($p < 0.0001$; Fig. 4A,B). Concurrently, myelin basic protein (MBP) myelin-positive regions expanded substantially in POL cohorts relative to SCI groups ($p < 0.0001$; Fig. 4C,D). Growth-associated protein 43 (GAP43)—a neuron-specific phosphoprotein abundantly localized in axonal growth cones—mediates axonal development, guidance, and synaptic plasticity. WB analysis confirmed POL intervention restored GAP43 protein expression post-SCI, further evidencing axonal regeneration ($p = 0.0427$; Fig. 4E,F). For all original WB images in Fig. 4E see the **Supplementary material**. Post-traumatic glial scarring presents a primary physiological barrier to axonal regeneration [25]. We consequently evaluated glial scar formation via glial fibrillary acidic protein (GFAP) and ionized calcium-binding adapter molecule 1 (IBA1) immunofluorescence in spinal tissues at 7/28 dpi. SCI controls exhibited dense microglial and astrocytic accumulation within lesion epicenters. POL administration markedly attenuated microglial and astrocytic scar formation in injury cores, with superior efficacy at higher doses ($p < 0.0001$; Fig. 4G–L). Collectively, these outcomes demonstrate POL treatment suppresses post-SCI glial cicatrization while facilitating axonal and myelin regeneration.

3.5 POL Treatment Attenuated Microglial-mediated Neuroinflammation After SCI

Following spinal cord injury, activated microglia propagate inflammatory mediators iNOS and COX-2 while

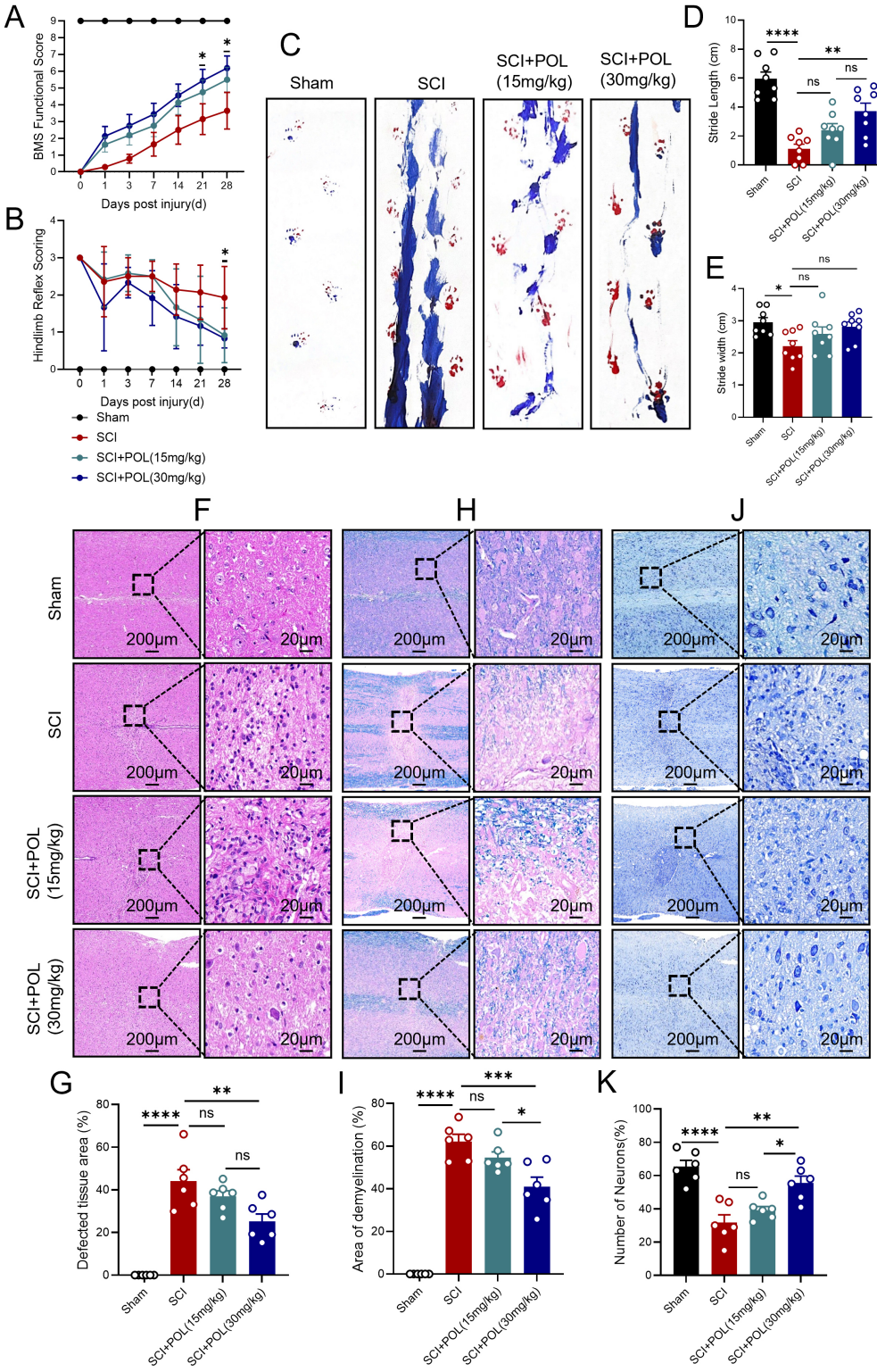

Fig. 2. POL treatment alleviated pathological changes and improved motor function after SCI. (A) BMS metrics within 28 dpi across sham, SCI, POL-treated SCI cohorts. (B) Hindlimb reflex metrics at 28 dpi. (C) Exemplar plantar imprints at 28 dpi. Quantitative stride length (D) and base width (E) analyses. (F) H&E-stained transverse sections (28 dpi). Scale bars = 200 μm, 20 μm. (G) Lesion area quantification. (H) LFB-stained longitudinal sections depicting myelination (28 dpi). Scale bars = 200 μm, 20 μm. (I) Demyelinated area quantification. (J) Nissl-stained longitudinal sections (28 dpi). Scale bars = 200 μm, 20 μm. (K) Surviving neuron quantification. Data: mean ± SEM; N = 6/group (3 experiments). Statistical determinations deployed one-way ANOVA with Tukey's post hoc analysis. *$p < 0.05$ vs SCI, **$p < 0.01$, ***$p < 0.001$, ****$p < 0.0001$, ns = non-significant.

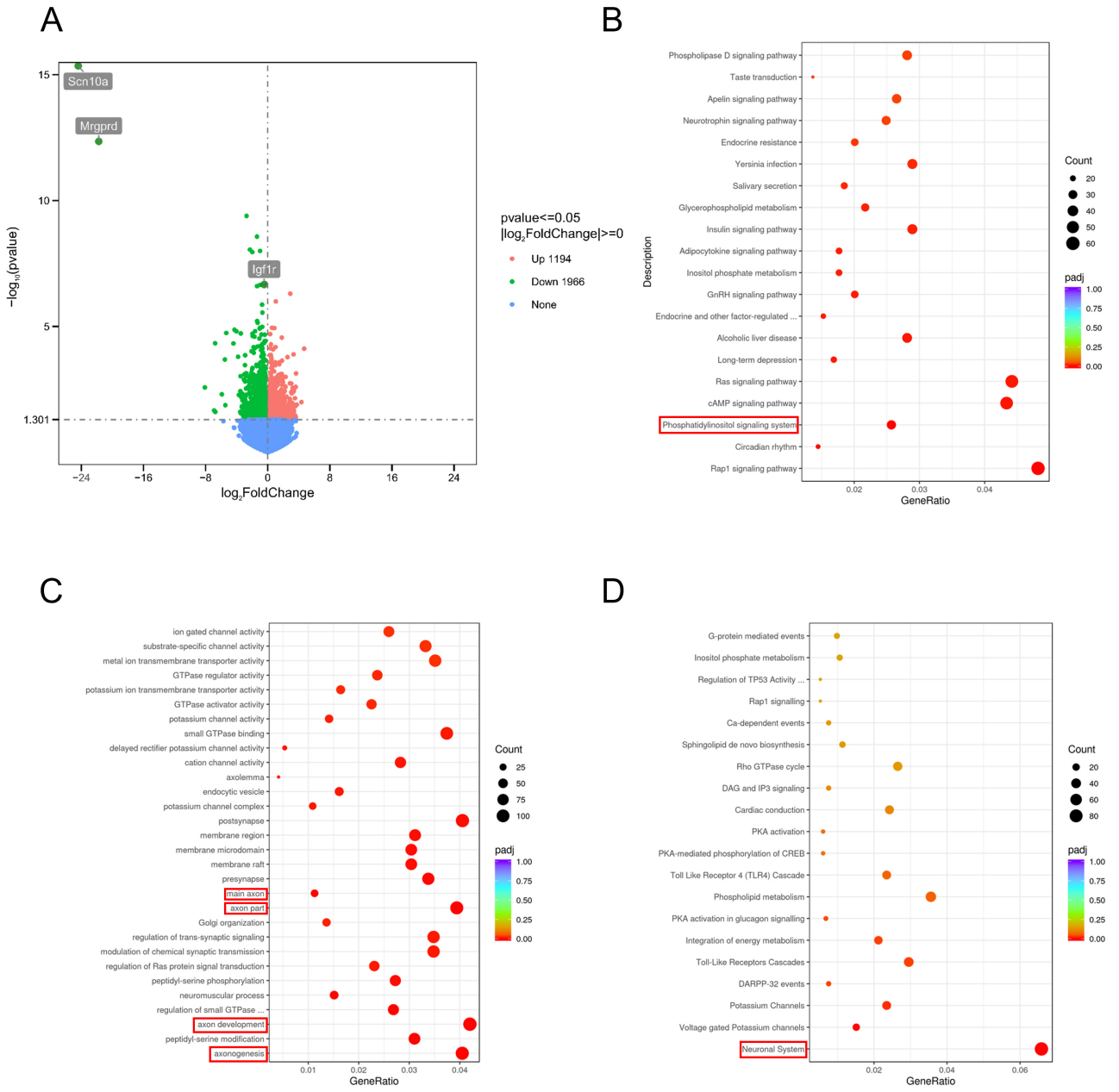

Fig. 3. POL treatment modulated gene expression and regulated axon regeneration-associated pathways after SCI. (A) Differential expression volcano map between SCI and SCI+POL cohorts. (B) KEGG pathway enrichment profiling. (C) Gene Ontology enrichment assessment. (D) Reactome pathway enrichment analysis. KEGG, Kyoto encyclopedia of genes and genomes. In panels B, C, and D, the red boxes highlight the KEGG pathway, GO term, and Reactome pathway, respectively, that were highly enriched and most directly related to the axon and neuroinflammation under investigation. In the three parentheses in the part of the figure references of the results, we have also added "red box" accordingly.

secreting cytokines TNF-α, IL-1β, and IL-6. WB quantification revealed elevated protein expression of iNOS, COX-2, TNF-α, IL-1β, and IL-6 post-SCI. Poliumoside intervention substantially attenuated all five inflammatory markers, demonstrating suppression of post-traumatic neuroinflammation (iNOS: $p = 0.0003$; COX-2: $p = 0.0019$; IL-1β: $p < 0.0001$; IL-6: $p < 0.0001$; TNF-α: $p = 0.0004$; Fig. 5A–F). For all original WB images in Fig. 5A see the

Supplementary material. Immunofluorescence corroborated POL's capacity to mitigate microglia-mediated neuroinflammation. Co-staining of microglial marker IBA1 with iNOS demonstrated reduced iNOS fluorescence intensity in IBA1-positive cells following POL administration versus injury controls ($p < 0.0001$; Fig. 5G,H). Additional co-localization studies of TNF-α/IL-1β and IL-6/COX-2 confirmed significantly diminished fluorescence intensities

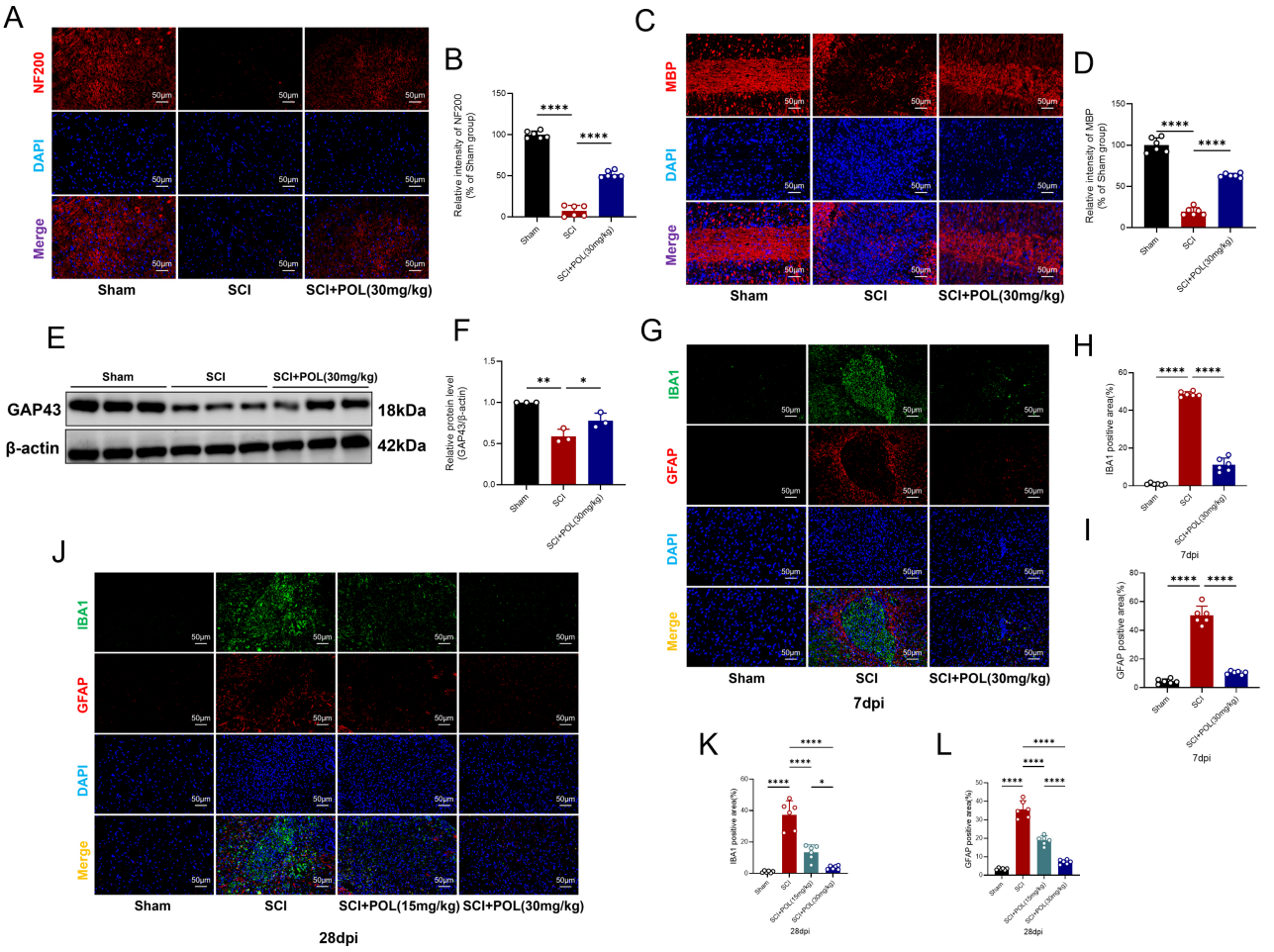

Fig. 4. POL treatment enhanced axonal regeneration and myelin repair while reducing glial scar after SCI. (A) NF200 axonal distribution (red) in longitudinal sections (7 dpi). Scale bar = 50 µm. (B) NF200 fluorescence quantification. (C) MBP myelination (red; 7 dpi). Scale bar = 50 µm. (D) MBP fluorescence quantification. (E) Representative GAP43 WB (3 dpi). (F) GAP43 expression quantification. (G,J) Dual IBA1 microglia (green)/GFAP astrocytes (red) immunofluorescence at 28 dpi (H) and 7 dpi (K). Scale bar = 50 µm. (H,K) IBA1 fluorescence quantification. (I,L) GFAP fluorescence quantification. Blot data: mean ± SEM; N = 3/group (3 experiments). Immunofluorescence data: mean ± SEM; N = 6/group (3 experiments). Statistics: one-way ANOVA + Tukey's post hoc. *$p < 0.05$ vs. SCI group, **$p < 0.01$, ****$p < 0.0001$. NF200, Neurofilament 200; GAP43, Growth-associated protein 43.

for all four markers in POL-treated cohorts relative to SCI groups (IL-1β: $p < 0.0001$; TNF-α: $p < 0.0001$; IL-6: $p < 0.0001$; COX-2: $p < 0.0001$; Fig. 5I–N). These collective findings establish POL's efficacy in alleviating microglial-driven neuroinflammatory responses post-SCI.

3.6 POL Treatment Attenuated Microglial-mediated Oxidative Stress After SCI

Compared to the injury cohort, POL administration post-SCI significantly mitigated levels of the oxidative stress-associated proteins NOX2 and NOX4 (NOX2: $p = 0.0406$; NOX4: $p = 0.0128$) (Fig. 6A–C). For all original WB images in Fig. 6A see the **Supplementary material**. The microglial biomarker IBA1 underwent concomitant staining with NOX4. Immunofluorescence analysis revealed POL substantially diminished NOX4 fluorescence intensity co-localized with IBA1 relative to injured controls (NOX4: $p < 0.0001$) (Fig. 6D,E). These observations indicate POL treatment alleviated microglial oxidative stress following spinal cord injury.

3.7 POL Treatment Suppressed LPS-induced Neuroinflammation in BV-2 Microglial Cells

BV-2 microglial cellular viability under varying POL dosages underwent assessment via CCK-8 methodology. Incubation with POL exclusively (5, 10, 20, 40, 80 µM) for 24 hours manifested no viability alterations (Fig. 7A). This investigation consequently elected 20 µM POL for ensuing cellular assays. LPS activation of BV-2 microglia *in vitro* replicated post-spinal cord injury neuroinflammatory cascades. WB analyses revealed LPS markedly amplified iNOS and COX-2 protein quantities, which POL

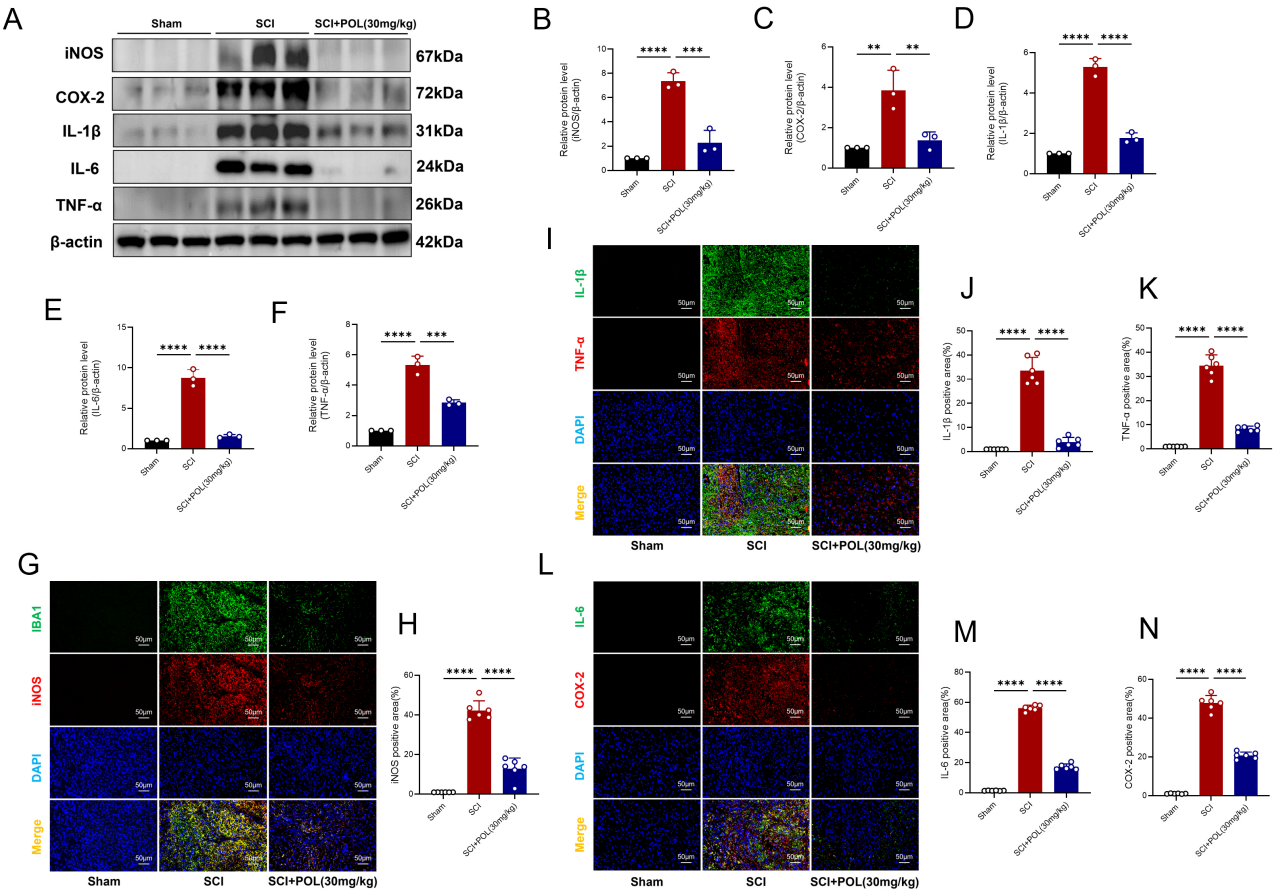

Fig. 5. POL treatment attenuated microglial-mediated neuroinflammation after SCI. (A) Representative iNOS, COX-2, IL-1β, IL-6, TNF-α WB (3 dpi). (B) iNOS quantification. (C) COX-2 quantification. (D) IL-1β quantification. (E) IL-6 quantification. (F) TNF-α quantification. (G) IBA1 (green)/iNOS (red) co-staining (7 dpi). Scale bar = 50 µm. (H) iNOS fluorescence quantification. (I) IL-1β (green)/TNF-α (red) co-staining (7 dpi). Scale bar = 50 µm. (J) IL-1β fluorescence quantification. (K) TNF-α fluorescence quantification. (L) IL-6 (green)/COX-2 (red) co-staining (7 dpi). Scale bar = 50 µm. (M) IL-6 fluorescence quantification. (N) COX-2 fluorescence quantification. Blot data: mean ± SEM; N = 3/group (3 experiments). IF data: mean ± SEM; N = 6/group (3 experiments). Statistics: one-way ANOVA + Tukey's post hoc. $^{**}p < 0.01$ vs. SCI group, $^{***}p < 0.001$, $^{****}p < 0.0001$.

administration substantially attenuated (iNOS: $p = 0.0388$; COX-2: $p = 0.0207$; Fig. 7B–D). For all original Western blot images in Fig. 7B see the **Supplementary material**. Immunofluorescence imaging demonstrated inflammatory markers iNOS and COX-2 intensification 6 hours post-LPS provocation. Following 20 µM POL intervention, LPS-induced iNOS levels declined (Fig. 7E), with COX-2 exhibiting analogous diminishment (Fig. 7F). These outcomes validate POL's neuroinflammation-inhibiting efficacy within microglia.

3.8 POL Treatment Activated the PI3K/AKT/mTOR Signaling Pathway After SCI

To delineate the precise molecular actions of POL against SCI, guided by RNA-Seq indications, molecular docking assessed POL's binding capacity towards three pivotal targets: PI3K, AKT, and mTOR, followed by evaluation of the PI3K/AKT/mTOR cascade both *in vivo* and *in vitro*. Docking simulations revealed substantial binding affinities between POL and core PI3K/AKT/mTOR constituents, exhibiting energies of –7.5 kcal/mol (PI3K), –8.8 kcal/mol (AKT), and –9.1 kcal/mol (mTOR), all surpassing the established threshold for potent molecular binding (<–7 kcal/mol) (Fig. 8A). Immunoblot analyses of spinal cord tissue demonstrated markedly diminished p-PI3K/PI3K, p-AKT/AKT, and p-mTOR/mTOR ratios at 3 dpi. Conversely, POL administration elevated these phosphorylated protein ratios significantly (p-PI3K/PI3K: $p = 0.0021$; p-AKT/AKT: $p = 0.0013$; p-mTOR/mTOR: $p = 0.0005$) (Fig. 8B–E). Analogously, within the microglial model, LPS challenge substantially reduced p-PI3K/PI3K, p-AKT/AKT, and p-mTOR/mTOR levels. POL treatment conversely augmented these ratios (p-PI3K/PI3K: $p = 0.0017$; p-AKT/AKT: $p = 0.0002$; p-mTOR/mTOR: $p = 0.0355$) (Fig. 8F–I). For all original WB images in Fig. 8B,F see the **Supplementary material**. These findings imply

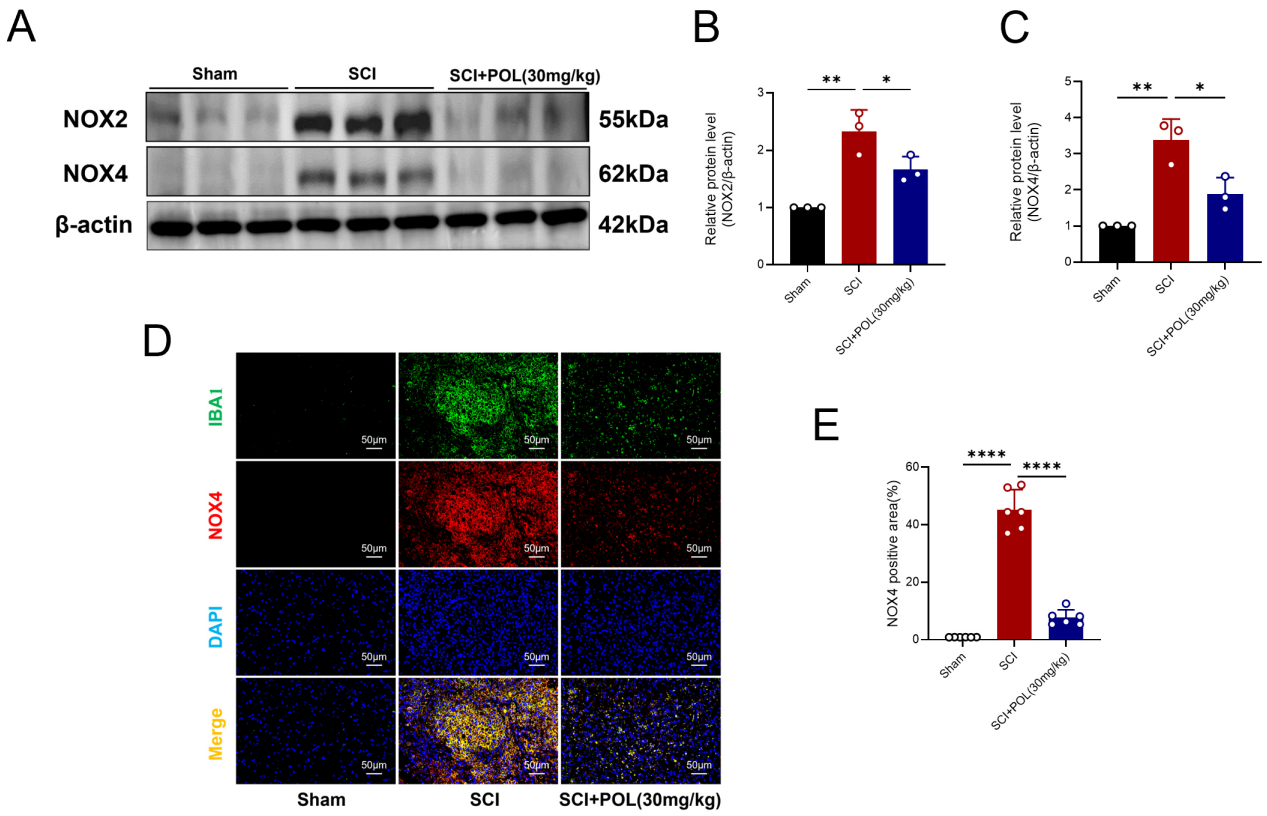

Fig. 6. POL treatment attenuated microglial-mediated oxidative stress after SCI. (A) Representative WB depict NOX2 and NOX4 levels within the spinal cord at 3 dpi. (B) Quantitative assessment of NOX2 expression. (C) Quantitative assessment of NOX4 expression. (D) Dual immunofluorescence labeling visualized microglia via IBA1 (green) and NOX4 (red) at 7 dpi. Scale bar = 50 μm. (E) Quantification of NOX4 fluorescence intensity. WB quantification reflects mean ± SEM derived from 3 independent experiments, each utilizing 3 mice per group (N = 3 per group). Immunofluorescence quantification presents mean ± SEM from 3 independent experiments, each employing 6 mice per group (N = 6 per group). Statistical significance was ascertained utilizing one-way ANOVA succeeded by Tukey's post hoc test. *$p < 0.05$ vs. SCI group, *$p < 0.05$, **$p < 0.01$, ****$p < 0.0001$.

POL's activation of the PI3K/AKT/mTOR signaling cascade post-SCI constitutes its principal therapeutic mechanism.

4. Discussion

SCI constitutes a devastating, persistent, irreversible disability marked by profound sensory and motor deficits [26]. SCI pathophysiology encompasses two discrete stages: primary mechanical damage and secondary injury—the latter denoting progressive pathological cascades initiated post-trauma, involving neuroinflammation, oxidative stress, motor neuron apoptosis, tissue edema, and blood-spinal cord barrier (BSCB) compromise [27]. Consequently, formulating effective early-stage therapeutic interventions to alleviate secondary injury remains imperative. This investigation initially establishes POL administration mediates neuroprotection and enhances functional restoration post-SCI through mitigation of inflammatory processes and oxidative damage. Specifically, *in vivo* POL treatment substantially diminished neuronal apoptosis, microglia-driven neuroinflammation, oxidative injury, demyelination, and glial scarring, while concurrently promoting axonal regrowth. *In vitro*, POL treatment attenuated LPS-induced microglial inflammatory reactions, aligning with prior observations [17]. Mechanistically, our evidence suggests POL likely orchestrates these safeguarding outcomes via PI3K/mTOR/AKT signaling pathway activation. Taken together, these discoveries furnish novel mechanistic understanding of POL's neuroprotective function during SCI recuperation, underscoring its early-intervention therapeutic promise.

POL, a phenylethanoid glycoside, possesses anti-inflammatory, antioxidant, anti-apoptotic, and neuroprotective properties [28]. Prior research examining Forsythoside B (a structural analog among phenylethanoid glycosides) for SCI management utilized animal doses of 10 mg/kg and 40 mg/kg [29]. Consequently, this investigation employed two analogous POL concentrations (15 mg/kg and 30 mg/kg) administered intraperitoneally. These doses also were consistent with those used in recent research

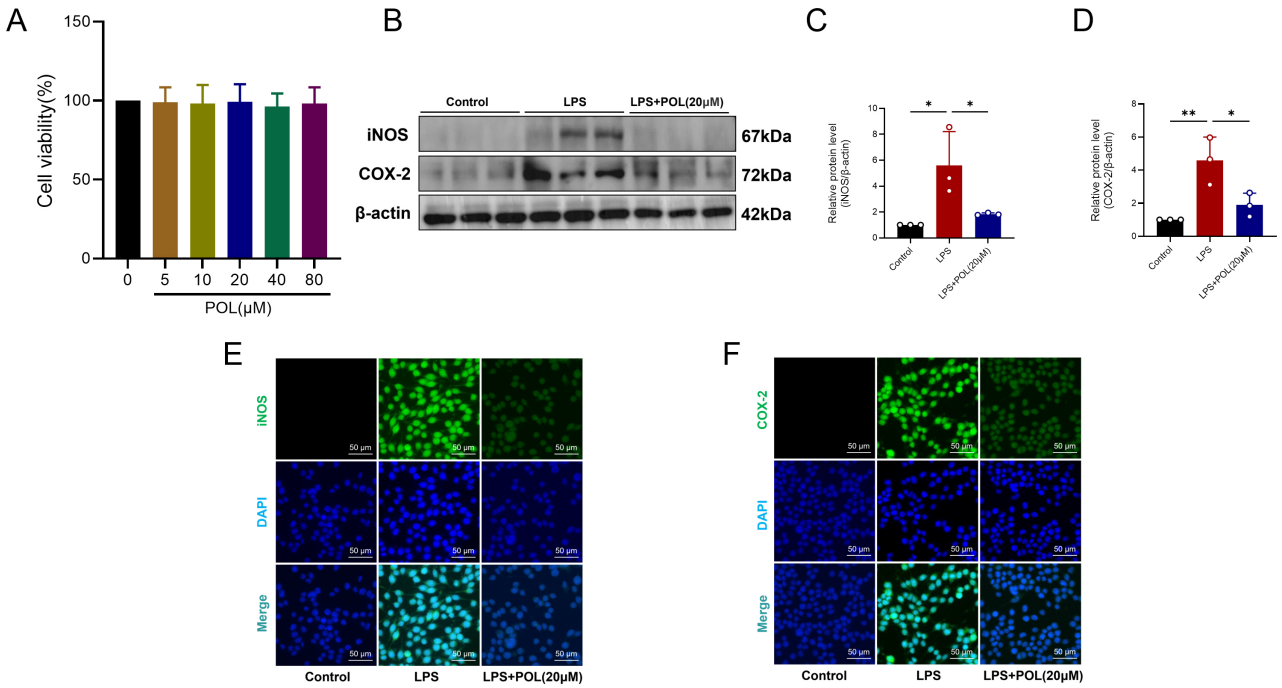

Fig. 7. POL treatment suppressed LPS-induced neuroinflammation in BV-2 microglial cells. (A) CCK-8 assay quantifying cellular viability. (B) Representative WB depicting iNOS/COX-2 levels in BV-2 microglia after 24-hour POL exposure and 6-hour LPS stimulation. (C) iNOS expression quantitative evaluation. (D) COX-2 expression quantitative evaluation. (E) Representative immunofluorescence visualizing iNOS (green) in BV-2 microglia post-treatment. Scale bar = 50 μm. (F) Representative immunofluorescence visualizing COX-2 (green) under identical conditions. Scale bar = 50 μm. CCK-8 data: mean ± SEM from triplicate independent experiments, each encompassing six BV-2 microglial cells per cohort (N = 6/group). WB quantifications: mean ± SEM from triplicate experiments, each comprising three BV-2 microglial cells per cohort (N = 3/group). Statistical significances were ascertained via one-way ANOVA with Tukey's post hoc analysis. *$p < 0.05$ vs. SCI group, *$p < 0.05$, **$p < 0.01$. LPS, Lipopolysaccharide; CCK-8, Cell Counting Kit-8.

that demonstrated POL's efficacy in mitigating microglia-mediated neuroinflammation after ischemic stroke at 5, 10, and 15 mg/kg doses [19]. Given the absence of prior toxicity data for POL, we first evaluated its systemic effects in healthy mice, particularly in CNS tissues. H&E staining confirmed the absence of toxicological effects at both 15 mg/kg and 30 mg/kg doses. Behavioral tests directly demonstrated the ability of POL treatment to enhance motor function recovery post-SCI, and histological analyses revealed reduced demyelination, increased neuronal survival, and diminished lesion areas. Notably, the 30 mg/kg dose exhibited significantly better therapeutic outcomes than did 15 mg/kg, which warranted its selection for subsequent experiments. Beyond established anti-inflammatory and antioxidant effects, RNA-Seq analysis was conducted to elucidate POL's mechanistic underpinnings in SCI. Results indicated POL's robust promotion of axonal regeneration and active involvement in nervous system biological processes, potentially mediated by downstream PI3K/AKT/mTOR pathway modulation.

Axons, constituting fundamental structural and operational units within neural circuitry, serve an indispensable function in neuronal signal transmission. Thus, injuries affecting either the central or peripheral nervous systems mandate axonal regrowth to reinstate neurological capabilities [30]. Axonal remodeling and regeneration represent pivotal determinants for neural network reconstitution following spinal cord trauma [31]. Substantial evidence indicates microglia-driven neuroinflammation and oxidative stress provoke liberation of neurotoxic agents post-SCI, subsequently yielding excessive glial proliferation, cicatrix formation, suppression of axonal regeneration, and exacerbation of neural tissue destruction [32,33], thereby impeding motor function recovery. These observations align with our experimental outcomes demonstrating POL treatment attenuated microglia-mediated neuroinflammation and oxidative stress after SCI, consequently inhibiting post-injury glial scar development while facilitating axonal regrowth and myelin restoration.

The PI3K/AKT/mTOR signaling cascade—comprising PI3K, AKT, and mTOR—serves as a master regulator of fundamental cellular processes including growth, proliferation, survival, and metabolic homeostasis [34]. Accumulating evidence underscores its neuroprotective potential following SCI [22,35]. For example, EX-netrin1 regulated inflammation and axon growth

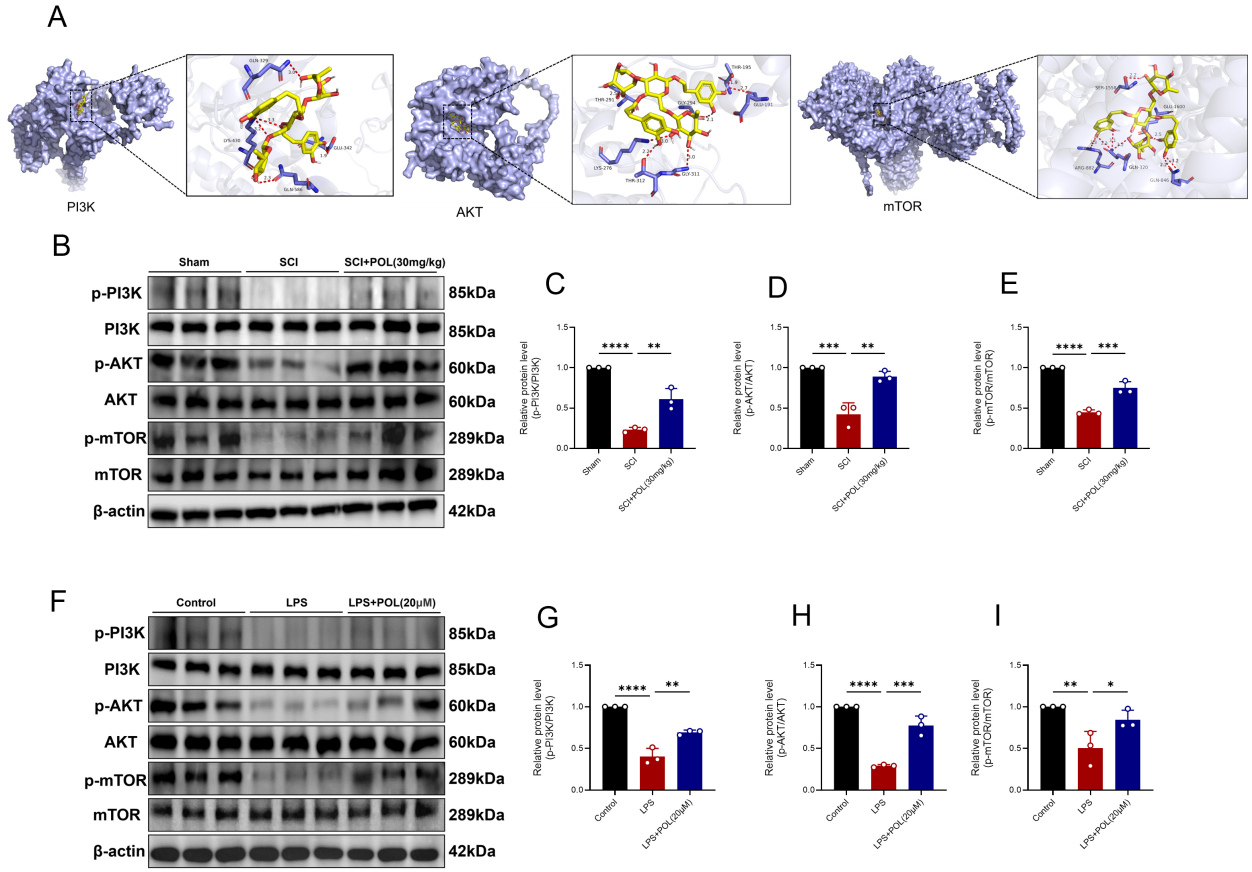

Fig. 8. POL treatment activated the PI3K/AKT/mTOR signaling pathway after SCI. (A) Molecular docking models depicting POL's binding interactions with PI3K, AKT, and mTOR. (B) Representative WB of phosphorylated and total PI3K/AKT/mTOR proteins in spinal cord tissue at 3 dpi. (C) Quantification of p-PI3K/PI3K expression levels. (D) Quantification of p-AKT/AKT expression levels. (E) Quantification of p-mTOR/mTOR expression levels. (F) Representative immunoblots depicting phosphorylation states and corresponding total PI3K, AKT, and mTOR proteins in BV-2 microglial cells following 24-hour POL administration and 6-hour LPS exposure. (G) Quantification of p-PI3K/PI3K expression levels. (H) Quantification of p-AKT/AKT expression levels. (I) Quantification of p-mTOR/mTOR expression levels; Findings are presented as mean ± SEM derived from three distinct experimental replicates, each encompassing three mice or BV-2 microglial cell samples per cohort (N = 3 per group). Statistical significance was assessed using one-way ANOVA with Tukey's post hoc analysis. *$p < 0.05$ vs. SCI group, *$p < 0.05$, **$p < 0.01$, ***$p < 0.001$, ****$p < 0.0001$. PI3K, phosphatidylinositol 3-kinase; AKT, protein kinase B; mTOR, mechanistic target of rapamycin.

after SCI via the Unc5b/PI3K/AKT/mTOR pathway [36]. Similarly, a neural regeneration-enhanced triple-network hydrogel promotes neuronal differentiation, inhibits astrocyte differentiation, and supports axonal regeneration via activating the PI3K/AKT/mTOR signaling pathway [37]. Our *in vivo* and *in vitro* findings corroborate these neurorestorative properties. Intriguingly, KEGG pathway enrichment analysis suggests that POL's therapeutic mechanism in SCI may also involve the Ras signaling pathway. Ras, a small GTP-binding protein, functions as a molecular switch at the cell membrane to initiate signaling cascades promoting cell growth and proliferation, with Raf kinase serving as its primary effector [38]. This is supported by recent work of serum response factor (SRF)-mediated axonal regeneration via Ras/Raf/cofilin signaling demonstrating [39]. Moreover, LNT-UsSeNPs directly regulated the PI3K/AKT/mTOR and Ras/Raf/MEK/ERK signaling pathways by regulating selenoproteins to achieve non-immunosuppressive anti-inflammatorytherapy [40]. Therefore, the potential involvement of POL in modulating the Ras signaling pathway opens a promising new avenue for comprehensively elucidating its therapeutic mechanisms in SCI.

Based on RNA-Seq results, we observed significant downregulation of *Igf1r*, an axonal regeneration-related target gene, following POL treatment. *Igf1r* encodes a transmembrane tyrosine kinase receptor orchestrating multifunctional participation within SCI pathophysiology, governing cell proliferation, survival, metabolic processes, and axonal regeneration [41]. Prior research established that combining twelve weeks of treadmill training with OPN overexpression enhanced axonal regeneration and motor

capabilities through activation of the IGF-1R/Akt/mTOR pathway. Analogously, we postulate that POL potentially activates the PI3K/AKT/mTOR signaling cascade by targeting *Igf1r*, thereby augmenting axonal regeneration; this offers crucial perspectives for discerning upstream therapeutic targets of POL in SCI management. Furthermore, *Scn10a* and *Mrgprd* constituted the two most substantially downregulated genes. Specifically, *Scn10a* encodes Nav1.8, a voltage-gated sodium channel exhibiting predominant expression within sensory neurons; within these neurons, Nav1.8 proves indispensable for generating and conducting action potentials. Nav1.8 plays a critical role in nociception due to its high expression in nociceptive neurons [42]. *Mrgprd* is primarily expressed in sensory neurons, particularly those mediating pain transmission, and functions to recognize and respond to specific neuropeptides and chemical substances that act as pain-signaling mediators [43]. In the chronic phase of SCI, approximately 90% of patients develop neuropathic pain below the injury level, significantly hindering rehabilitation [44]. Given that persistent inflammation across spinal segments contributes to post-SCI neuropathic pain, it is worth further investigating whether POL alleviates neuropathic pain by targeting *Scn10a* and *Mrgprd* and whether this effect is linked to its anti-inflammatory properties.

However, this study also has some limitations. First, in the cell experiments, we only verified the therapeutic effect of POL on BV2-mediated neuroinflammation, but did not explore the oxidative stress phenotype at the cellular level. Second, the optimal drug concentration of POL in cell experiments was not studied in detail. And last, the activation of the PI3K/AKT/mTOR signaling pathway was only simply verified; its association with neuroinflammation, oxidative stress, and axonal regeneration was not verified with a rescue experiment. Therefore, the directions for future research are whether POL affects other biological processes and related targets related to SCI, as well as other specific regulatory mechanisms related to POL's regulation of axonal regeneration. Subsequent investigations will examine combinations of POL with hydrogels, emerging nanomaterials, stem cells, and additional therapeutic agents to assess drug targeting efficacy and optimize delivery systems; relevant clinical trials will be integrated to accelerate clinical translation.

5. Conclusions

POL administration mitigated neuroinflammation and oxidative stress consequent to murine SCI through activation of the PI3K/AKT/mTOR signaling cascade. Furthermore, POL intervention diminished glial scar extent within injury epicenters while stimulating axonal regeneration and myelin restoration. Consequently, POL therapy enhances post-SCI motor function and facilitates neural functional recovery.

Availability of Data and Materials

The data during the research are available from the corresponding author on reasonable request.

Author Contributions

QL conceived and designed the study, performed the experiments, and drafted the manuscript. HH and GX contributed to the study design. MX and TW were responsible for data collection. ZZ and JH carried out data analysis. QF contributed to the experimental design, provided suggestions and assistance in establishing the mouse model of SCI, and participated in the preparation and organization of the figures. ZC made substantial contributions to the conception and design, provided critical revision of the manuscript for important intellectual content, and approved the final version. All authors contributed to editorial changes in the manuscript. All authors read and approved the final manuscript. All authors have participated sufficiently in the work and agreed to be accountable for all aspects of the work.

Ethics Approval and Consent to Participate

The animal study was reviewed and approved by the Animal Experiment Ethics Committee of Nantong University (No. S20250318-004) and use Committee and the National Institutes of Health Guide for the Care and Use of Laboratory Animals.

Acknowledgment

We would like to express our gratitude to all the reviewers for their constructive suggestions for this research.

Funding

This research was funded by Project of Jiangsu Administration of Traditional Chinese Medicine (No. MS2024092, MS2022090) and Jiangsu Provincial Health Commission Project (No. ZQ2024026).

Conflict of Interest

The authors declare no conflict of interest.

Supplementary Material

Supplementary material associated with this article can be found, in the online version, at https://doi.org/10.31083/JIN43900.

References

[1] Hu X, Xu W, Ren Y, Wang Z, He X, Huang R, *et al*. Spinal cord injury: molecular mechanisms and therapeutic interventions. Signal Transduction and Targeted Therapy. 2023; 8: 245. https://doi.org/10.1038/s41392-023-01477-6.

[2] Ding W, Hu S, Wang P, Kang H, Peng R, Dong Y, *et al*. Spinal Cord Injury: The Global Incidence, Prevalence, and Disability From the Global Burden of Disease Study 2019. Spine. 2022; 47: 1532–1540. https://doi.org/10.1097/BRS.0000000000004417.

[3] Sterner RC, Sterner RM. Immune response following traumatic spinal cord injury: Pathophysiology and therapies. Frontiers in Immunology. 2022; 13: 1084101. https://doi.org/10.3389/fimmu.2022.1084101.
[4] Hellenbrand DJ, Quinn CM, Piper ZJ, Morehouse CN, Fixel JA, Hanna AS. Inflammation after spinal cord injury: a review of the critical timeline of signaling cues and cellular infiltration. Journal of Neuroinflammation. 2021; 18: 284. https://doi.org/10.1186/s12974-021-02337-2.
[5] Gaire BP, Choi JW. Critical Roles of Lysophospholipid Receptors in Activation of Neuroglia and Their Neuroinflammatory Responses. International Journal of Molecular Sciences. 2021; 22: 7864. https://doi.org/10.3390/ijms22157864.
[6] Prinz M, Jung S, Priller J. Microglia Biology: One Century of Evolving Concepts. Cell. 2019; 179: 292–311. https://doi.org/10.1016/j.cell.2019.08.053.
[7] Fu SP, Chen SY, Pang QM, Zhang M, Wu XC, Wan X, *et al*. Advances in the research of the role of macrophage/microglia polarization-mediated inflammatory response in spinal cord injury. Frontiers in Immunology. 2022; 13: 1014013. https://doi.org/10.3389/fimmu.2022.1014013.
[8] Pang QM, Chen SY, Xu QJ, Fu SP, Yang YC, Zou WH, *et al*. Neuroinflammation and Scarring After Spinal Cord Injury: Therapeutic Roles of MSCs on Inflammation and Glial Scar. Frontiers in Immunology. 2021; 12: 751021. https://doi.org/10.3389/fimmu.2021.751021.
[9] Yu M, Wang Z, Wang D, Aierxi M, Ma Z, Wang Y. Oxidative stress following spinal cord injury: From molecular mechanisms to therapeutic targets. Journal of Neuroscience Research. 2023; 101: 1538–1554. https://doi.org/10.1002/jnr.25221.
[10] Timofeeva AV, Akhmetzyanova ER, Rizvanov AA, Mukhamedshina YO. Interaction of microglia with the microenvironment in spinal cord injury. Neuroscience. 2025; 565: 594–603. https://doi.org/10.1016/j.neuroscience.2024.11.074.
[11] Hilton BJ, Husch A, Schaffran B, Lin TC, Burnside ER, Dupraz S, *et al*. An active vesicle priming machinery suppresses axon regeneration upon adult CNS injury. Neuron. 2022; 110: 51–69.e7. https://doi.org/10.1016/j.neuron.2021.10.007.
[12] Elmalky MI, Alvarez-Bolado G, Younsi A, Skutella T. Axonal Regeneration after Spinal Cord Injury: Molecular Mechanisms, Regulatory Pathways, and Novel Strategies. Biology. 2024; 13: 703. https://doi.org/10.3390/biology13090703.
[13] He ZD, Lau KM, Xu HX, Li PC, Pui-Hay But P. Antioxidant activity of phenylethanoid glycosides from Brandisia hancei. Journal of Ethnopharmacology. 2000; 71: 483–486. https://doi.org/10.1016/s0378-8741(00)00189-6.
[14] Guo ZY, Li P, Huang W, Wang JJ, Liu YJ, Liu B, *et al*. Antioxidant and anti-inflammatory caffeoyl phenylpropanoid and secoiridoid glycosides from Jasminum nervosum stems, a Chinese folk medicine. Phytochemistry. 2014; 106: 124–133. https://doi.org/10.1016/j.phytochem.2014.07.011.
[15] Tian XY, Li MX, Lin T, Qiu Y, Zhu YT, Li XL, *et al*. A review on the structure and pharmacological activity of phenylethanoid glycosides. European Journal of Medicinal Chemistry. 2021; 209: 112563. https://doi.org/10.1016/j.ejmech.2020.112563.
[16] Zheng JN, Zhuo JY, Nie J, Liu YL, Chen BY, Wu AZ, *et al*. Phenylethanoid Glycosides From Callicarpa kwangtungensis Chun Attenuate TNF-α-Induced Cell Damage by Inhibiting NF-κB Pathway and Enhancing Nrf2 Pathway in A549 Cells. Frontiers in Pharmacology. 2021; 12: 693983. https://doi.org/10.3389/fphar.2021.693983.
[17] Zuo Y, Chen B, Li X, Liu G. Poliumoside inhibits apoptosis, oxidative stress and neuro-inflammation to prevent intracerebroventricular Streptozotocin-induced cognitive dysfunction in Sprague-Dawley Rats: in in-vivo, in-vitro and in-silico study. Folia Morphologica. 2025; 84: 359–370. https://doi.org/10.5603/fm.101463.
[18] Bai L, Guan Z, Zhang J, Lv Z, Duan Y, Tian S. Poliumoside Exhibits Neuroprotective Effects against Cerebral Ischemia-Reperfusion Injury by Relieving Microglia-Mediated Neuronal Damage and Astrocytic Activation. ACS Chemical Neuroscience. 2025; 16: 1780–1791. https://doi.org/10.1021/acschemneuro.4c00846.
[19] Gao Y, Wang J, Zhang C, Wang H, Wang B, Zhang X. Poliumoside alleviates microglia-mediated inflammation and blood-brain barrier disruption via modulating the polarization of microglia after ischemic stroke in mice. Phytomedicine: International Journal of Phytotherapy and Phytopharmacology. 2025; 143: 156881. https://doi.org/10.1016/j.phymed.2025.156881.
[20] Xia M, Li C, Chen J, Wu C, Zhang J, Hong H, *et al*. Activation of FANCC attenuates mitochondrial ROS-driven necroptosis by targeting TBK1-dependent mitophagy in astrocytes after spinal cord injury. Theranostics. 2025; 15: 4188–4211. https://doi.org/10.7150/thno.109071.
[21] Zhang J, Yang D, Huang H, Sun Y, Hu Y. Coordination of Necessary and Permissive Signals by PTEN Inhibition for CNS Axon Regeneration. Frontiers in Neuroscience. 2018; 12: 558. https://doi.org/10.3389/fnins.2018.00558.
[22] Xiao CL, Yin WC, Zhong YC, Luo JQ, Liu LL, Liu WY, *et al*. The role of PI3K/Akt signalling pathway in spinal cord injury. Biomedicine & Pharmacotherapy = Biomedecine & Pharmacotherapie. 2022; 156: 113881. https://doi.org/10.1016/j.biopha.2022.113881.
[23] Ding Y, Chen Q. mTOR pathway: A potential therapeutic target for spinal cord injury. Biomedicine & Pharmacotherapy = Biomedecine & Pharmacotherapie. 2022; 145: 112430. https://doi.org/10.1016/j.biopha.2021.112430.
[24] Basso DM, Fisher LC, Anderson AJ, Jakeman LB, McTigue DM, Popovich PG. Basso Mouse Scale for locomotion detects differences in recovery after spinal cord injury in five common mouse strains. Journal of Neurotrauma. 2006; 23: 635–659. https://doi.org/10.1089/neu.2006.23.635.
[25] Tran AP, Warren PM, Silver J. The Biology of Regeneration Failure and Success After Spinal Cord Injury. Physiological Reviews. 2018; 98: 881–917. https://doi.org/10.1152/physrev.00017.2017.
[26] McDonald JW, Sadowsky C. Spinal-cord injury. Lancet (London, England). 2002; 359: 417–425. https://doi.org/10.1016/S0140-6736(02)07603-1.
[27] Hilton BJ, Moulson AJ, Tetzlaff W. Neuroprotection and secondary damage following spinal cord injury: concepts and methods. Neuroscience Letters. 2017; 652: 3–10. https://doi.org/10.1016/j.neulet.2016.12.004.
[28] Wu L, Georgiev MI, Cao H, Nahar L, El-Seedi HR, Sarker SD, *et al*. Therapeutic potential of phenylethanoid glycosides: A systematic review. Medicinal Research Reviews. 2020; 40: 2605–2649. https://doi.org/10.1002/med.21717.
[29] Xia M, Zhang Y, Wu H, Zhang Q, Liu Q, Li G, *et al*. Forsythoside B attenuates neuro-inflammation and neuronal apoptosis by inhibition of NF-κB and p38-MAPK signaling pathways through activating Nrf2 post spinal cord injury. International Immunopharmacology. 2022; 111: 109120. https://doi.org/10.1016/j.intimp.2022.109120.
[30] Tomé D, Almeida RD. The injured axon: intrinsic mechanisms driving axonal regeneration. Trends in Neurosciences. 2024; 47: 875–891. https://doi.org/10.1016/j.tins.2024.09.009.
[31] Zheng B, Tuszynski MH. Regulation of axonal regeneration after mammalian spinal cord injury. Nature Reviews. Molecular Cell Biology. 2023; 24: 396–413. https://doi.org/10.1038/s41580-022-00562-y.
[32] Orr MB, Gensel JC. Spinal Cord Injury Scarring and Inflammation: Therapies Targeting Glial and Inflammatory Responses.

Neurotherapeutics: the Journal of the American Society for Experimental NeuroTherapeutics. 2018; 15: 541–553. https://doi.org/10.1007/s13311-018-0631-6.

[33] Shafqat A, Albalkhi I, Magableh HM, Saleh T, Alkattan K, Yaqinuddin A. Tackling the glial scar in spinal cord regeneration: new discoveries and future directions. Frontiers in Cellular Neuroscience. 2023; 17: 1180825. https://doi.org/10.3389/fncel.2023.1180825.

[34] Glaviano A, Foo ASC, Lam HY, Yap KCH, Jacot W, Jones RH, *et al*. PI3K/AKT/mTOR signaling transduction pathway and targeted therapies in cancer. Molecular Cancer. 2023; 22: 138. https://doi.org/10.1186/s12943-023-01827-6.

[35] He X, Li Y, Deng B, Lin A, Zhang G, Ma M, *et al*. The PI3K/AKT signalling pathway in inflammation, cell death and glial scar formation after traumatic spinal cord injury: Mechanisms and therapeutic opportunities. Cell Proliferation. 2022; 55: e13275. https://doi.org/10.1111/cpr.13275.

[36] Lu X, Xu G, Lin Z, Zou F, Liu S, Zhang Y, *et al*. Engineered exosomes enriched in netrin-1 modRNA promote axonal growth in spinal cord injury by attenuating inflammation and pyroptosis. Biomaterials Research. 2023; 27: 3. https://doi.org/10.1186/s40824-023-00339-0.

[37] Yun Z, Wu J, Sun X, Yu T, Xue W, Dai A, *et al*. Neural-enhancing PRP/Alg/GelMA triple-network hydrogel for neurogenesis and angiogenesis after spinal cord injury via PI3K/AKT/mTOR signaling pathway. Theranostics. 2025; 15: 3837–3861. https://doi.org/10.7150/thno.109091.

[38] Jeon H, Tkacik E, Eck MJ. Signaling from RAS to RAF: The Molecules and Their Mechanisms. Annual Review of Biochemistry. 2024; 93: 289–316. https://doi.org/10.1146/annurev-biochem-052521-040754.

[39] Gao L, Zhang C, Zhu Y, Zhang N, Zhang C, Zhou S, *et al*. Serum response factor promoting axonal regeneration by activating the Ras-Raf-Cofilin signaling pathway after the spinal cord injury. CNS Neuroscience & Therapeutics. 2024; 30: e14585. https://doi.org/10.1111/cns.14585.

[40] Liu P, Liu X, Wu Z, Shen K, Li Z, Li X, *et al*. Size effect-based improved antioxidant activity of selenium nanoparticles regulating Anti-PI3K-mTOR and Ras-MEK pathways for treating spinal cord injury to avoid hormone shock-induced immunosuppression. Journal of Nanobiotechnology. 2025; 23: 17. https://doi.org/10.1186/s12951-024-03054-7.

[41] Zhao XM, He XY, Liu J, Xu Y, Xu FF, Tan YX, *et al*. Neural Stem Cell Transplantation Improves Locomotor Function in Spinal Cord Transection Rats Associated with Nerve Regeneration and IGF-1 R Expression. Cell Transplantation. 2019; 28: 1197–1211. https://doi.org/10.1177/0963689719860128.

[42] Yang Q, Wu Z, Hadden JK, Odem MA, Zuo Y, Crook RJ, *et al*. Persistent pain after spinal cord injury is maintained by primary afferent activity. The Journal of Neuroscience: the Official Journal of the Society for Neuroscience. 2014; 34: 10765–10769. https://doi.org/10.1523/JNEUROSCI.5316-13.2014.

[43] Wang LB, Su XJ, Wu QF, Xu X, Wang XY, Chen M, *et al*. Parallel Spinal Pathways for Transmitting Reflexive and Affective Dimensions of Nocifensive Behaviors Evoked by Selective Activation of the Mas-Related G Protein-Coupled Receptor D-Positive and Transient Receptor Potential Vanilloid 1-Positive Subsets of Nociceptors. Frontiers in Cellular Neuroscience. 2022; 16: 910670. https://doi.org/10.3389/fncel.2022.910670.

[44] Widerström-Noga E. Neuropathic Pain and Spinal Cord Injury: Management, Phenotypes, and Biomarkers. Drugs. 2023; 83: 1001–1025. https://doi.org/10.1007/s40265-023-01903-7.